Superconductor Science and Technology

PAPER

Performance of layer wound epoxy-impregnated coils made from a multifilamentary cable of exfoliated YBCO

To cite this article: Vyacheslav Solovyov *et al* 2019 *Supercond. Sci. Technol.* **32** 054006

IOP Publishing Superconductor Science and Technology
Supercond. Sci. Technol. 32 (2019) 054006 (14pp) https://doi.org/10.1088/1361-6668/ab0b9c

Performance of layer wound epoxy-impregnated coils made from a multifilamentary cable of exfoliated YBCO

Vyacheslav Solovyov[1], Saad Rabbani[1], Monan Ma[1,2], Zachary Mendleson[1,2], Timothy Haugan[3] and Paul Farrell[1]

[1] Brookhaven Technology Group Inc., Advanced Energy Research and Technology Center, 1000 Innovation Road, Stony Brook, NY 11794, United States of America
[2] Stony Brook University, Stony Brook, NY 11794, United States of America
[3] Aerospace Systems Directorate, Wright-Patterson Air Force Base, OH 45433-7251, United States of America

E-mail: slowa@brookhaventech.com

Received 30 October 2018, revised 14 February 2019
Accepted for publication 28 February 2019
Published 12 April 2019

Abstract

The performance and reliability of magnets made from second generation (2G), exfoliated, YBCO conductors are highly improved by use of narrow, stacked, multifilamentary cable instead of a single wide tape. This paper reports on tests of five mini-coils wound from 2.4 mm wide ExoCable™, which is comprised of eight, stacked, exfoliated, YBCO filaments. The filaments are coupled electrically through a re-flow process, which results in enhanced electrical connectivity between the adjacent layers. The coils were tested at 77 K (up to 500 A) in liquid nitrogen and at 22 K (up to 700 A) in a conduction-cooled mode. The cable carries 500 A critical current at 77 K. A six-layer coil wound from 10.5 m of the cable, the largest coil created in the study, demonstrates a critical current of 280 A at 77 K at 0.4 T magnetic field on the winding. The coils were fully impregnated with Stycast 1266 and Henkel W19 low-viscosity epoxies. Repeated thermal cycling, to 77 and 22 K, does not degrade the coil's performance. The cable AC loss and the coil winding magnetization are compared with the traditional 2G wide tape pancake geometry at 77 K. We observe a five times reduction of the winding magnetization when the 12 mm tape is replaced by a 2.4 mm cable, which is explained by the smaller magnetic moment of the cable winding. The field hysteresis profiles recorded at 22 and 77 K are presented to demonstrate the effect of the operation temperature on the winding magnetization. A finite element analysis of the winding magnetization shows a good agreement between the experimentally measured trapped field value, and the critical state model prediction. Finally, we discuss the stability of an ExoCable™ coil in a conduction-cooled operation.

Keywords: 2G conductors, magnet coils, epoxy impregnation, YBCO

(Some figures may appear in colour only in the online journal)

1. Introduction

Second generation (2G) coated high temperature superconductors are traditionally manufactured and marketed as high-aspect ratio (thin and wide) tapes [1, 2]. This conductor geometry is incompatible with traditional, continuous, layer wound magnets. Instead, 2G magnets are comprised of a series of connected pancake coils. The pancakes are wound from a single wide filament stabilized by a thin, $<100\,\mu$m, layer of copper. Several groups have demonstrated high-field solenoids made of single-filament 2G pancake stacks [3], but it is recognized that protecting these magnets from destructive quenches is difficult. A thin layer of copper stabilizer provides little passive protection, at typical operating currents, $>500\,\mathrm{A\,mm^{-2}}$, whereas slow propagation of the normal zone, $\approx 1\,\mathrm{cm\,s^{-1}}$ [4], necessitates highly advanced active quench protection system. So-called

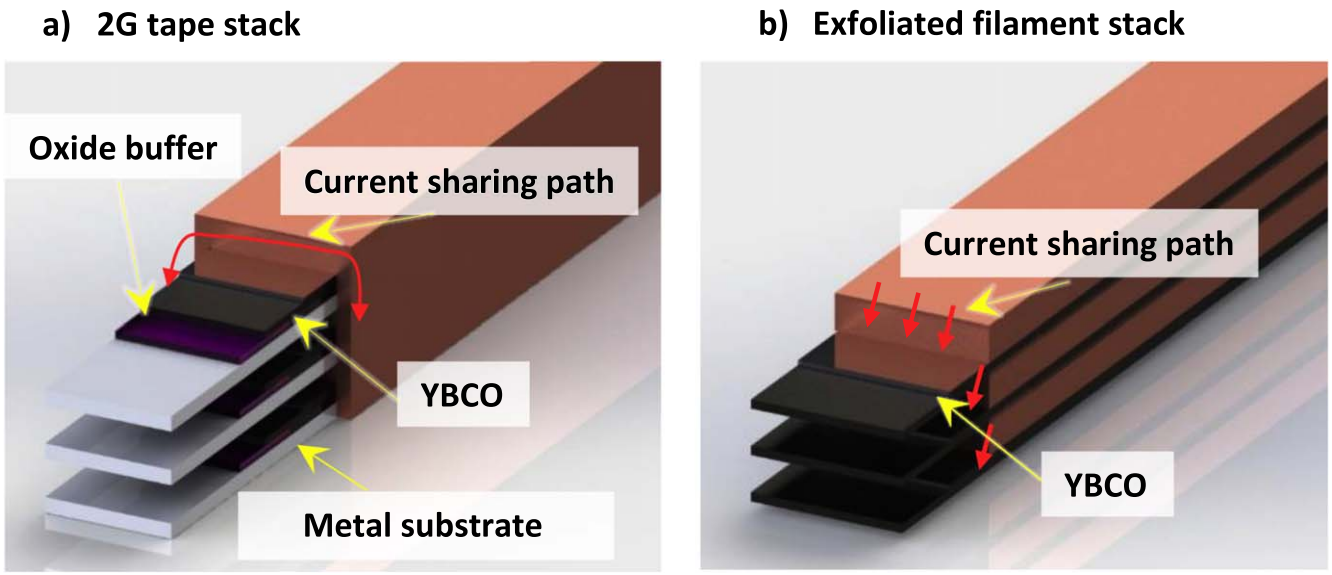

Figure 1. (a) Current sharing in a 2G tape stack. Only lateral current sharing is possible due to current blocking by the substrate. (b) Current sharing in the exfoliated filament stack. The arrows indicate direction of the sharing current flow.

no-insulation (NI) magnets [5, 6] emerged recently as a promising way to introduce current sharing between adjacent layers of a pancake in order to enhance the magnet stability. The NI approach revealed several drawbacks, such as a very low allowable ramping rate and long field settling time.

A thin, <1 mm, multistrand, electrically coupled cable can potentially enable a stable, fast ramping magnet with acceptable field quality and low magnetization loss. In a multifilamentary cable architecture, a local perturbation of superconductivity is moderated by transfer of the current to neighboring filaments. Currently several cabling approaches, such as twisted stack [7, 8], spiral-wound cable [9] and Roebel cable [10] are being explored.

Using traditional laminated 2G tapes in a cable does not address the issue of poor current sharing between layers because the oxide buffer between layers blocks normal (perpendicular to the tape face) current transfer. Thus, addition of extra metal on the sides of the stack is required to provide a path for lateral current flow, as shown in figure 1(a). In order to provide meaningfully low resistance for the current flow, the side metal needs to be thick, which limits the practical cable width in this approach up to 3–4 mm. Poor current sharing can be mitigated by improved uniformity of constituting filaments [11], which, however, raises the cable cost. This is because manufacturing defect-free continuous coupons of 2G tape has proven very difficult. After over 20 years of the technology's development, the typical coupon length offered by the leading 2G tape producers is $\approx$100 m. Longer coupons are sold at a premium.

In this work, we report on use of the recently developed ExoCable™, which is a new YBCO filament architecture [12], in a set of small magnet coils. Because the substrate is removed, normal current transfer can be realized by simply bonding the filaments in a vertical stack, see figure 1(b). Normal current transfer between adjacent layers enables a narrow electrically coupled cable that is tolerant to local defects. Several test coils were made and characterized to demonstrate the following salient features of the technology: (i) short, <10 mm current transfer length; (ii) layer winding; (iii) compatibility with low-viscosity epoxy impregnation; (iv) simplified current and voltage lead connection.

2. Experimental details and digital methods

Commercially available 10 mm wide 2G tapes were exfoliated following a procedure described in [12]. The exfoliated tapes were sliced into 2.4 mm wide filaments using a 200 W CO_2 laser. The laser lens had a focal length of 2.5″ (Kern Lasers HSE model), figure 2(a). The supplied laser processing table was equipped with a custom tape motion and positioning system. Additionally, a digital camera was attached to the laser head for positioning and quality control. The laser slicing system was operated via a LabVIEW code that synchronizes the laser head motion with the tape advance.

Assist gas allowed for efficient evacuation of the cut product. The gas was delivered under pressure though a 1 mm diameter nozzle. The assist gas also served to cool the surrounding areas. The laser head was coupled to a height follower system that maintains the lens tip at 100 μm distance above the filament. Cooling by the assist gas had proven to be especially critical for preventing the solder layer inside the exfoliated filament from melting. The typical cutting speed for a 75 μm copper-supported filament was 2 cm s^{-1}.

The filaments were coated with Sn62Pb36Ag02 solder by a reel-to-reel dip coating process. We note that the same solder was used to attach current and voltage leads. Prior to the solder coating, the filament entered a flux bath filled with 2331-ZX flux (Kester Illinois Tool Works Company). The solder coating was performed at a 1 cm s^{-1} tape speed with a solder bath temperature of 240 °C. The coated filaments were arranged in a stacked array as shown in figures 2(b), (c). In

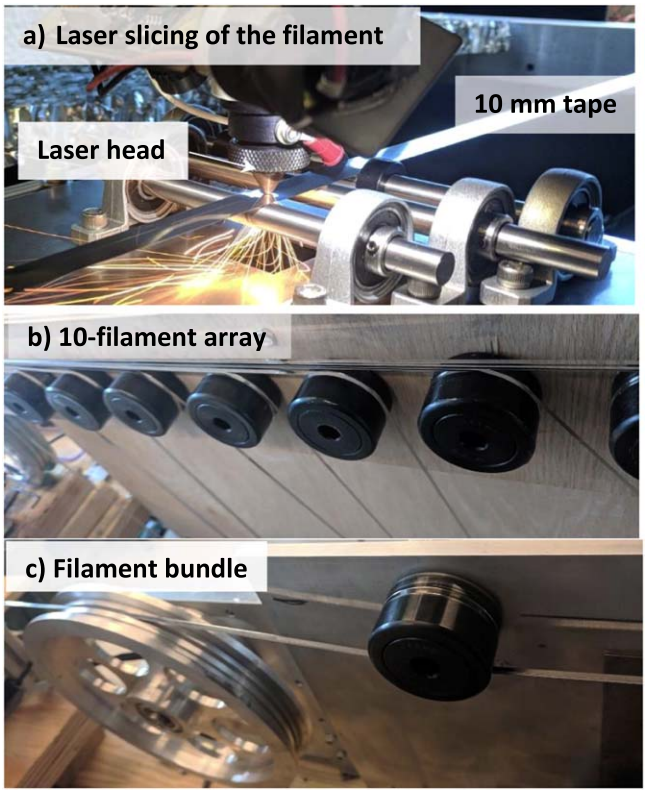

Figure 2. (a) Detail of the laser slicing arrangement, showing the laser head and the tape support. (b) 10-filament array prepared for bundling; (c) 10-filmanent bundle entering the wrapping machine.

this experiment, the cable was comprised of eight 2.4 mm wide YBCO filaments sandwiched between two 2.38 mm wide, 0.16 mm thick Nichrome ribbons[4]. The total cable thickness was thus approximately 1.2 mm. The stack comprised of eight YBCO filaments and two outer Nichrome ribbons (see figure 3(a)) was wrapped with 40 AWG Nichrome wire with 2 mm pitch. Figure 3(a) shows the partially separated stack. The inner YBCO filaments and the Nichrome cladding are clearly visible.

High-frequency AC losses of short, 10 cm, cable coupons were evaluated at a high-field calorimetric loss measurement system [13]. Briefly, AC loss was measured at 0.6 T alternating magnetic field generated by rotating permanent magnets. The field frequency was varied from 10 to 100 Hz by changing the rate of revolution of the permanent magnet rotor. Prior to each run, the system was calibrated using a fixed resistor heated by DC current. The calibration curve allowed determining the dissipated power level from the rate of nitrogen gas boil-off.

The cable was wound around an 80 mm diameter G10 tube under 10 N tension. The G10 tube determined the standard test coil dimensions in this study to be 80 mm internal diameter, 60 mm height. The current leads were made by soldering the YBCO filament stack to a 200 μm thick, 30 mm long copper foil tab. Then, 3 mm braided copper wires were soldered to the tab, thus finishing the current lead. The Nichrome wire wrap prevented the cable turns from directly touching each other, thus providing partial insulation. The voltage leads were 32 AWG polytetrafluoroethylene-insulated wires (Alpha wire) directly soldered to the edge of the superconducting filament stack, as shown in figure 3(e).

The coil assembly was placed in a furnace for the re-flow step. The optimum re-flow temperature is determined by differential-scanning calorimetry (DSC) of the ExoCable™ filaments using DSC Q2000 instrument (TA Instruments). During the re-flow, the solder coating of the YBCO filaments partially melted, thus fusing the filaments into an electrically and mechanically coupled solid, as shown in figures 3(b), (c). Figure 3(d) shows an *as-wound* six-layer coil, mounted on a 77 K critical current measurement setup. After characterization of the *as-wound* coil at 77 K, the same set of measurements was repeated after the re-flow and epoxy impregnation steps. The transport current was provided by Sorensen 10/1200 power supply, the coil voltage was measured by Keithley 182 nano-voltmeter. For the fast Fourier transform measurements, the coil signal was amplified by a Stanford Research SR 560 amplifier and digitally processed by a National Instrument 9205 module operating as a part of real-time signal processing system.

A traditional double-pancake coil was wound on the same G10 former for comparative magnetization tests at 77 K. The coil, wound from 12 turns of SuperPower 12 mm wide tape, had the same field constant as a single layer cable coil. The pancake coil was not epoxy-impregnated.

Low-viscocity epoxies, Stycast 1266 and Henkel Loctite Stycast W19 with Catalyst 11 (Ellsworth Adhesives), were used for the winding impregnation. The coils were wrapped with six layers of 5 mil fiberglass and placed in a tight-fitting moldfilled with epoxy. The mold was evacuated in a vacuum chamber for 20 min, after which the epoxy was cured following the manufacturer recommended curing profile. The fully impregntaed six-layer test coil with current and volatage leads attached is shown in figure 3(e).

Figure 4 is a photograph of the 22 K conduction-cooled (cryogen-free) test setup. The coil was cooled via a copper collar, which was directly attached to a single-stage cryo-cooler (CryoMech model AL230). The current leads were made from multistrand brass cable. One of the current leads was connected directly to the cryo-cooler head, where another lead was insulated from the cryo-cooler with a 50 μm thick Kapton film. The setup was rated for 700 A maximum current at 22 K. Several T-type thermocouples monitored temperature of the current leads and the cooling plate. Additionally, a thermocouple was embedded into the winding of a coil during the epoxy impregnation process to observe the winding temperature.

In both 77 and 22 K setups the magnetic field, generated by the coil was measured by miniature Ga–As Hall sensors (HG372A-ND, by ATK semiconductors). The sensors were calibrated against a factory-calibrated cryogenic Hall probe (FW Bell). Finite element analysis of the winding magnetization and thermal stress were carried out in COMSOL 5.2a environment. Both models were axial symmetric. The electromagnetic model was based on the original work by Ainslie *et al* [14].

[4] Hyndman Industries, 3/32 inch wide, 0.0063 inch thick, standard Kanthal A1 ribbon.

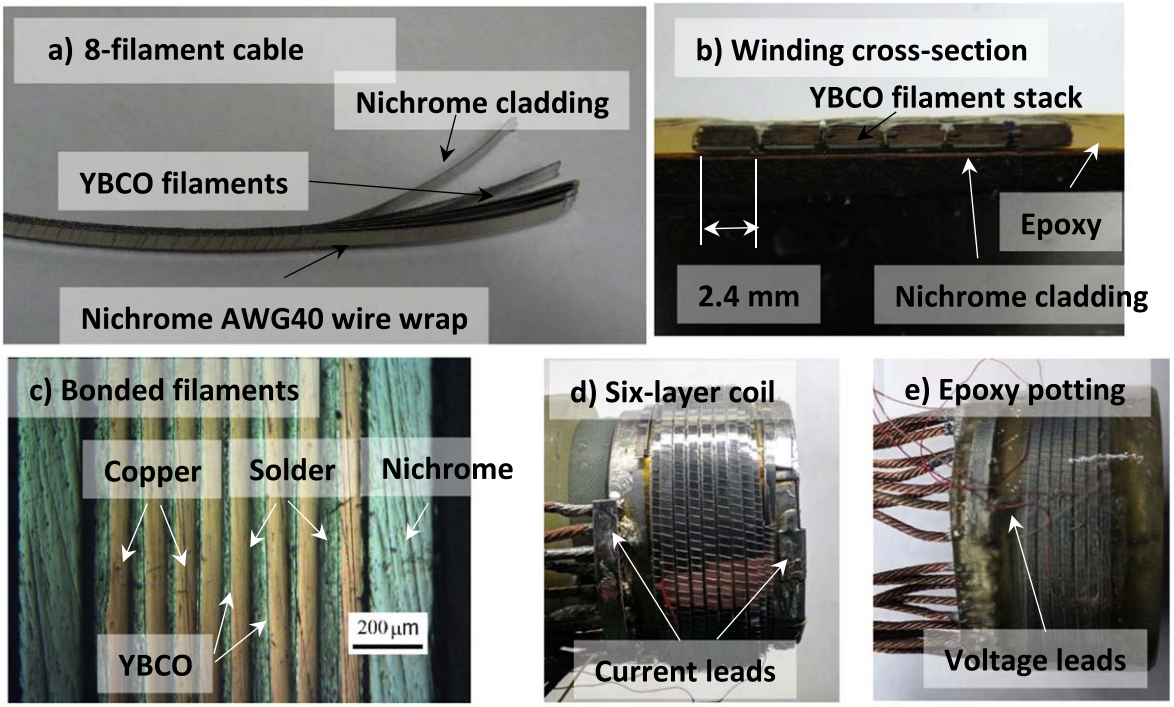

Figure 3. Test coil manufacturing process. (a) Photograph of the eight-filament cable coupon. (b) Cross-section of a one-layer epoxy-impregnated winding. (c) Optical micrograph of bonded exfoliated filaments showing copper stabilizer, solder coating, Nichrome wrap and position of the YBCO layer. (d), (e) The six-layer test coil (sample C3, table 1) before (d) and after (e) impregnation with fiberglass-reinforced Stycast 1266 epoxy.

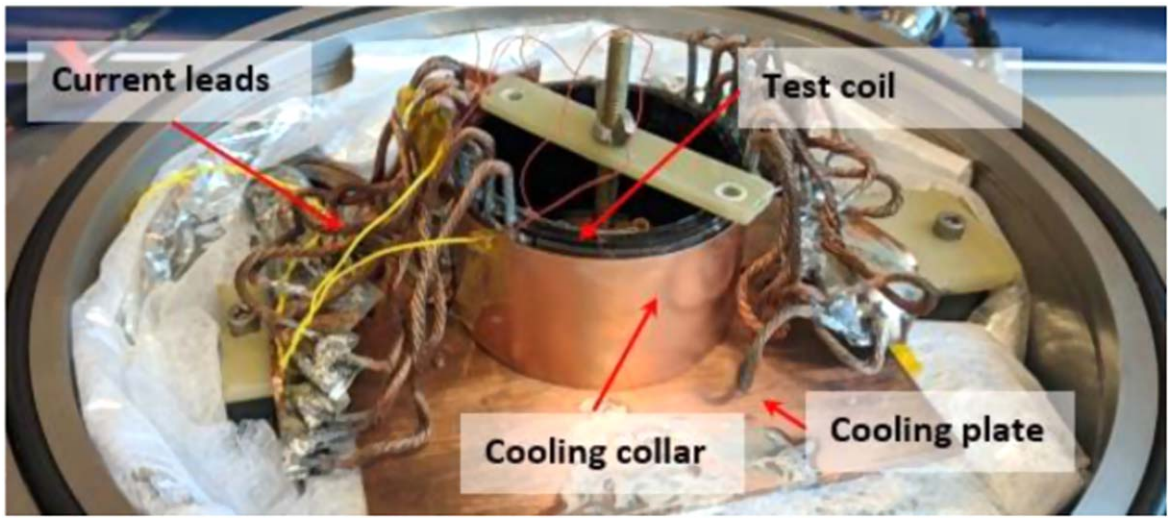

Figure 4. The 22 K coil test, conduction-cooled mode. The setup was cooled by CryoMech AL230 cryo-cooler (not shown).

3. Results

3.1. Laser filament slicing

Laser slicing enables manufacturing of narrow filaments but carries a penalty of heat damage to the material in the vicinity of the cut. The extent of the damage is quantified as the width of the head damage zone (HDZ) [15]. The exfoliated ExoCable™ filaments are sensitive to overheating because the solder attaching the YBCO layer to copper stabilizer melts at approximately 180 °C. After the solder melts and re-solidifies the surface tension effects result in regularly spaced wrinkles in the YBCO layer, or striations, clearly seen in figure 5(a). For a 2 mm wide filament, shown in figure 5(a), the heat-induced striations occupy approximately a 1 mm wide band, or 50% of the filament area. SEM micrographs presented in figures 5(d), (e), show microscopic detail of the striation. The edge view in figures 5(d), (e) shows that within a striation, the YBCO layer is sharply buckled to a height of $\sim$10 μm. We found that filaments with extensive striations exhibit suppressed and non-uniform critical current.

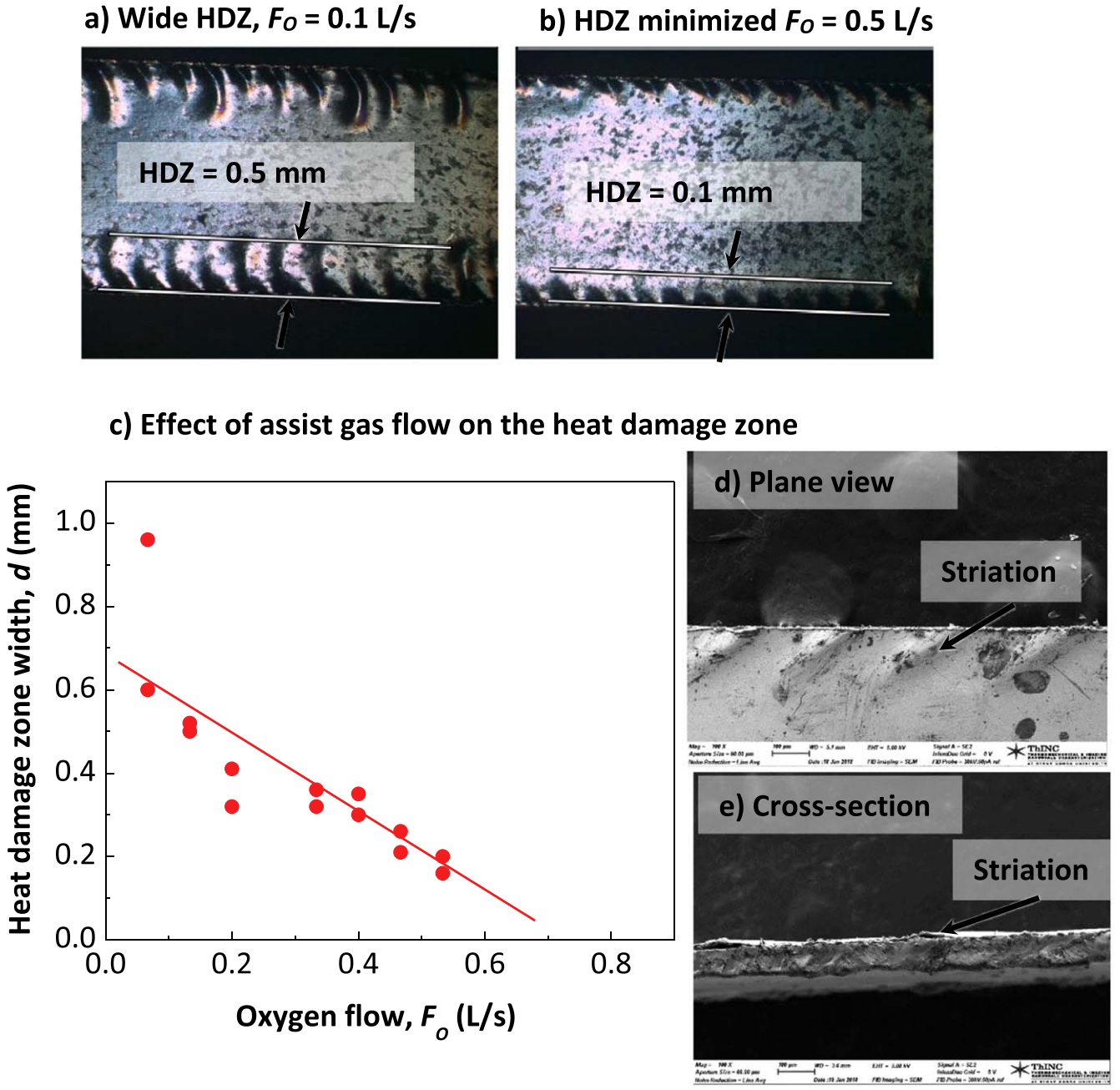

Figure 5. (a) Optical micrograph of the edge damage to 2 mm wide exfoliated filaments due to the laser beam overheating. (b) The head damage zone is minimized by the cutting optimization. (c) Dependence of the heat damage zone width on the assist gas flow rate. (d), (e) Scanning electron micrographs of the filament edge showing details of the YBCO layer striation.

The length of the striation is steadily reduced as the deposited energy is decreased. Replacing nitrogen with oxygen as the assist gas allows further reduction of the laser energy and further reduction of the HDZ width. This is because oxygen assists cutting through chemical oxidation of the melt, thus an equivalent cut rate can be achieved at a lower deposited energy. However, in the current configuration the laser does cut the tape at deposited energy level below 2 J cm^{-1}. As shown in figure 5(c), the edge damage is gradually reduced as the assist gas flow is increased, which is explained by cooling of the cut edge by the assist gas flow. Figure 5(b) is the optical micrograph of a filament cut under both optimized laser power and 1.5 l s^{-1} oxygen gas flow. The filament surface clearly shows significant reduction of the edge striation length and width of HDZ.

Figure 6 presents an of I_c versus filament width dependence for exfoliated filaments sliced with the CO_2 laser. The dashed rectangle shows the level of the original I_c for the 10 mm wide tape. The solid lines are best fit approximations by the following function which described dependence of I_c of a filament of width w, assuming that the edge damage zones of width, d, are non-superconducting:

$$I_c(w) = I_c(1 - 2d/w). \quad (1)$$

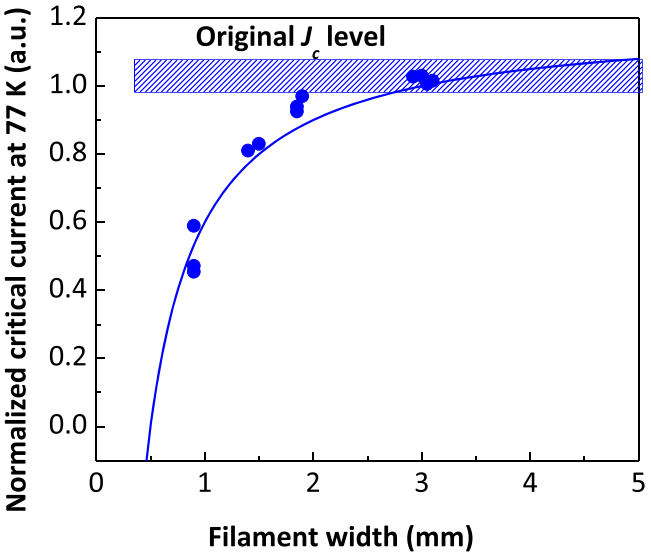

Figure 6. Dependence of the critical current density on the filament width. The solid lines represent best fits using equation (1).

Here, the fitting parameter d predicts that when $w = 2d$, the edge damage zones would overlap, and the effective critical current would be zero. The approximations show that for filaments sliced with the CO_2 and CW fiber lasers, $d = 200 \pm 20\ \mu$m. This is consistent with the optical measurement data presented in figure 5. On average, laser-sliced 2.4 mm wide filaments retain ~85% of the critical current of a 10 mm wide tape.

3.2. Solder coating, re-flow and filament bonding

Solder re-flow is critical for positive and reliable electrical coupling between filaments. The filament surface, especially close to the laser cut edge is uneven, therefore relatively thick solder coating of 20–40 μm is needed to fill the gaps between filaments. Figure 7(a) presents dependence of the coating thickness on the tape advance speed at three solder bath temperatures. Faster moving tape has less time to come to a temperature equilibrium with the solder bath, thus collecting more solder. Higher temperature delivers better and thinner solder coatings, but at the same time, it increases the possibility of solder completely de-alloying the silver coating. The optimized coating conditions, 1 cm s^{-1} tape speed and solder temperature 240 °C delivered 40 μm solder coating without degradation of the critical current density.

The optimum re-flow temperature ensures connectivity between filaments while maintaining the integrity of the silver coating. The recommended re-flow temperature of 225 °C [16] for Sn–Pb eutectics adapted by the electronics industry is too high for the 1 μm silver coating. During our trials, the silver coating de-alloyed within a second when dipped into 225 °C eutectic solder. Therefore, the DSC method to detect the end of the melting event of the coated filament was used, and the re-flow temperature was set as low as possible.

Figure 7(b) compares DSC profiles for uncoated and coated filaments. The re-flow temperature of 185 °C, which is at the end of the solder coating melting event, is chosen. The optimum re-flow duration was determined by measurement of

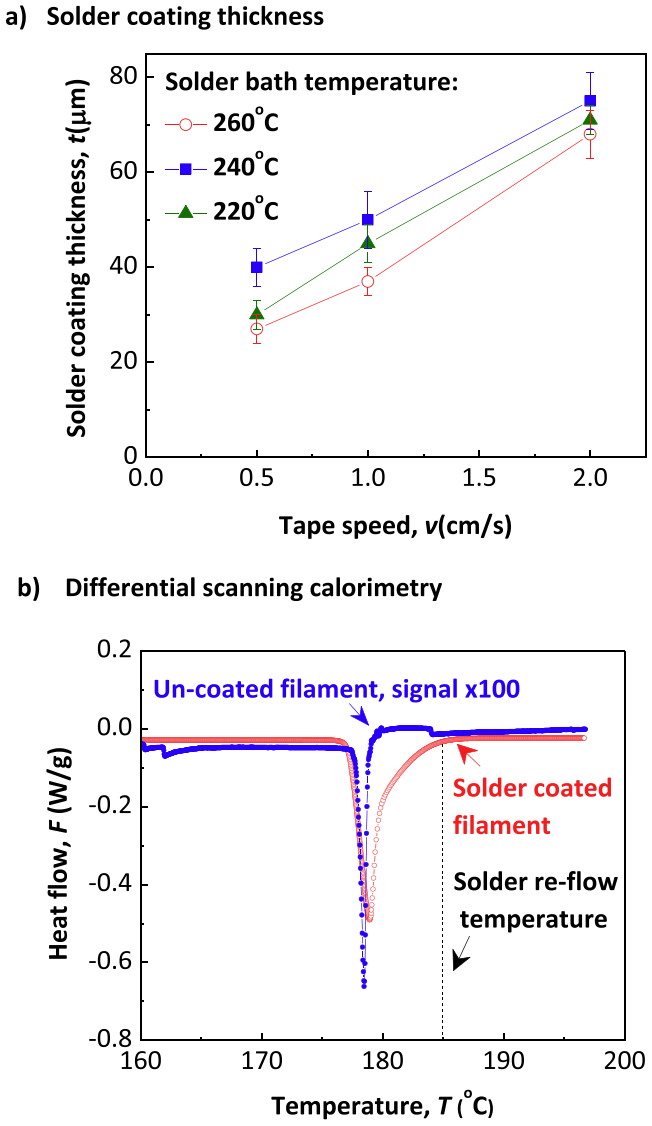

Figure 7. Solder coating and re-flow optimization. (a) Dependence of the solder coating thickness on the tape speed for various solder bath temperatures. (b) DSC signal for the uncoated filament and a filament coated with Sn62Pb36Ag02 solder. The temperature profile shows a distinct feature at 180 °C associated with the solder melting. The solder re-flow temperature, indicated as the dashed vertical line, was selected at the very end of the meting event. The uncoated filament signal was multiplied by a factor of 100 to account for the difference in the solder coating mass.

inter-filament contact resistivity (see figure 8). At 185 °C, the inter-filament contact resistivity reached the minimum of 400 nΩ cm^2 after 10 min of heat treatment. The re-flow temperature proved to be very critical for reliable filament bonding. Too low a temperature, <182 °C delivered little melting and poor connectivity, while at 190 °C and higher, the silver layer is rapidly de-alloyed and the critical current starts to degrade rapidly.

3.3. Coil tests

Table 1 provides a summary of test coil measurements. Here, the critical current values correspond to 77 K I_c in the

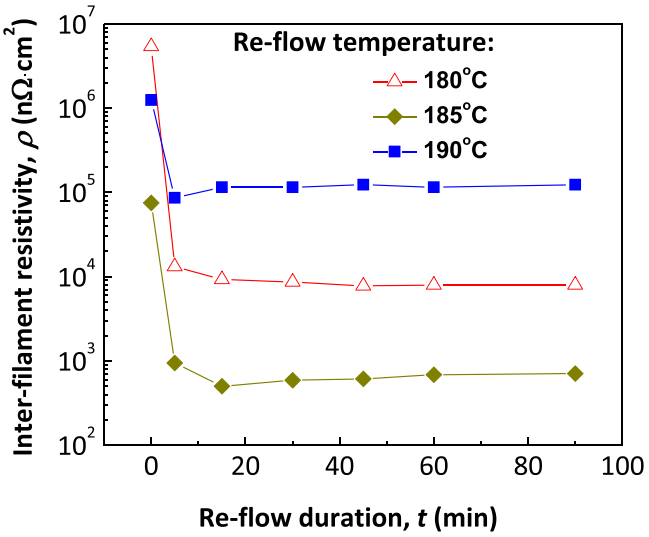

Figure 8. Dependence of the inter-filament contact resistivity on the re-flow temperature and the re-flow duration.

self-field. All the coils, except for C1, are re-enforced with six layers of fiberglass wrap. The field constant for the coils are: 1.2×10^{-4} T A^{-1} for a one-layer coil, 2.1×10^{-4} T A^{-1} for the three-layer coil and 5.2×10^{-4} T A^{-1} for the six-layer coil. The calculated self-field value on the winding reached 0.4 T for the six-layer coil at 77 K. The field values are approximately 1.75 times higher at 22 K when the coils were tested up to 700 A, which was the limit of the current leads in the 22 K conduction-cooled system.

Figure 9 illustrates the process of optimization of current leads for the coils. As already mentioned, unlike traditional 2G cables, the ExoCable™ can be soldered to a normal metal lead, such as copper, without separating the filaments, as shown in figure 9(a). The objective of the lead design optimization is a configuration where the current density within the lead area does not exceed I_c of the cable due to a local current build up. In a simplest lead design, one side of the cable is soldered to a copper plate (see upper panel of figure 9(a)). Figure 9(b) shows that such a single-side injection is not sufficient to distribute the current evenly, as the cable show signs of normal transition at 300 A. Doubling the lead length, from 15 to 30 mm results in a marginal improvement. By sandwiching the stack between two copper tabs, lower panel of figure 9(a), the current lead resistance is improved by a factor of two and the onset of the normal transition increases to 480 A, which is the critical current of the cable. In this configuration the current is injected into both sides of the YBCO filament stack, thus the current is distributed more evenly.

We estimated the current transfer length of the cable by recording *I–V* curved with 1 cm intervals from the current leads. The curves coincided with each other, indicating that the current transfer length of the cable is below 10 mm. Since insulation was not used, the winding turns were partially shorted by touching the Nichrome wire wrap. The coil inductance was thus determined from the frequency, f, dependence of the absolute impedance, $|Z|$, which allowed separating the active parts of the impedance from the reactive part. A typical dependence of the winding impedance (coil C2) is shown in figure 10. The simplified equivalent circuit of the coil is presented as the inset in figure 10. Briefly, the coil is modeled as series resistance R_s, the equivalent inductance L and parallel resistance R_p. Here R_p represents inter-layer and inter-turn resistance, which was in the range of 50–100 mΩ for all the test coils. The best fit of the experimental data with the impedance of the equivalent circuit is shown as a solid line. The inductance value, 6.2 ± 0.3 μH is in reasonable agreement with the value calculated from the finite element magneto-static model, 5.3 μH. Except for multilayer coils, the inductance values listed in table 1 were measured experimentally. The procedure did not work well for higher inductance multilayer coil because the equivalent circuit analysis can be applied in the high-inductance case only over a very limited frequency range. We note, that the calculated and experimentally measured inductance values coincided within 5%.

Figures 11(a) and (b) summarizes the effect of solder re-flow and epoxy impregnation on 77 K *I–V* curves of six-layer and three-layer coils. On average, solder-re-flow reduced the critical current by $8\% \pm 4\%$. The epoxy impregnation reduced I_c on $2\% \pm 0.5\%$. Figure 11(c) documents tolerance of the coils to thermal cycling. In the experiment, the coils were rapidly submersed in liquid nitrogen thus delivering the maximum thermal shock. Only coil C1, which was not reinforced with fiberglass, exhibits the initial I_c reduction. Inspection of the coil revealed a crack running across the winding, see inset in figure 11(c). We note, however, that further cycling does not degrade the coil performance.

A notable effect of solder-reflow is a significant reduction of the winding noise. The winding noise manifests itself as rapid spikes of voltage when the transport current is applied to the winding. This can be clearly seen in the *I–V* curve of the *as-wound* coil in figure 11(b). The noise is especially prominent in a large coil, such as six-layer C3. We observe at least ×100 reduction of noise after the re-flow step and no change after impregnation. To eliminate a possibility of mechanical motion, we prepared a coil sample, C4 without the re-flow step. The winding noise remained unchanged, which eliminated the winding vibration as a source.

Figure 12 quantifies effect of the solder re-flow by comparing Fourier spectra of winding signal of sample C2 after winding, figure 12(a), and after the solder-reflow, figure 12(b). The noise, responsible for the voltage jumps has a very wide spectrum; notably, there are low-frequency excitations at ≈0.1 Hz. The Fourier harmonics power increases by ≈200 after the transport current is applied. After the re-flow-step the noise level increases only marginally after the transport current application, figure 12(b).

3.4. AC loss and winding magnetization

Figure 13 compares the AC loss of short, 10 cm, coupons of the cable with 4 and 12 mm wide *SuperPower* tape measured at 0.6 T, 100 Hz. The loss value is normalized by the critical current thus leaving only the filament size contribution. The

Table 1. Summary of test coil parameters. The data labeled with * were obtained through a FEM simulation. The rest are experimentally measured.

ID	Description	Meters of cable	*n*-value	I_c(A) as-wound	I_c(A) after re-flow	I_c(A) after impregnation	$L(\mu H)$	$\mu_0 H(T)$ *at* 77 K *center*
S1	Straight coupon	0.2	25	495	497			
C1	One layer	2.0	21	498	425	362	5.2	0.06
C2	Three layers	4.5	20	418	394	380	27*	0.11
C3	Six layers	10.5	16	322	298	291	145*	0.18
C4	One layer, no Re-flow	1.8	18	425	N/A	425	4.8	0.12
C5	One layer, W19 epoxy	1.8	20	430	410	408	4.5	0.11

linear approximation, represented as a straight line, demonstrates reduction of AC loss in the 2.4 mm cable compared with 4 and 12 mm tapes. The inset presents dependency of AC on the magnetic field frequency in 10–100 Hz range. The solid line is a linear approximation, intended to emphasize that the loss mechanism is magnetization with negligible coupling and eddy current contribution.

On the coil level, a detailed comparison of winding magnetization was carried out by measuring the Hall signal hysteresis at 2 cm (half radius) distance from the coil center. Figure 14(a) presents a magnetic field hysteresis of the one-layer coil, sample C5, after the first ramp to 200 A, and subsequent ramps. As expected, the first ramp produces the largest trapped field. The subsequent ramps represent partial hysteresis curves superimposed on magnetization acquired by the winding in the first ramp. Figure 14(b) demonstrates the reduction of winding magnetization achieved by replacing a traditional 12 mm wide tape with a 2.4 mm ExoCable™ cable. Here, the hysteresis was normalized by the maximum magnetic field value, thus allowing for superposition of data from coils with different numbers of turns. The normalized hysteresis is a dimensionless measure of field quality (or field error), which can be realized by a conductor in a given geometry. Figure 14(c) presents the magnetic field hysteresis of coil C5 at 22 K. We observe a little change in the hysteresis magnitude between 77 and 22 K, as shown in the summary, figure 14(d). The high Hall sensor noise in figure 14(c) is due to mechanical vibration of the cryo-cooler.

4. Discussion

4.1. Narrow filament slicing

The present design is that of a compact, electrically coupled cable, compatible with low-viscosity epoxy impregnation. The narrow, electrically stable exfoliated ExoCable™ filament is the key element of the design. Narrow, preferably <1 mm wide filaments, have multiple benefits such as reduced AC loss, improved field quality and better stability [17]. Our approach is accomplished through use of laser slicing of the filaments, as opposed to chemical or mechanical patterning of the superconducting layer into parallel stripes [18].

Transitioning from 12 to 4 mm wide tape, that is currently offered by the industry to narrower filaments, required development of a laser slicing procedure that is compatible with the heat-sensitive nature of exfoliated YBCO. In this study we use readily available and well-established CO_2 laser technology. Unfortunately, the continuous wave operation mode of the CO_2 laser imposes a high heat load on the material, necessitating cooling of the cut edge with high flow of assist gas (see figure 5). At the gas flow rate of $0.5\,l\,s^{-1}$ used in the experiment, a standard industrial gas tank emptied in 2 h. The wavelength of CO_2 laser, 10.6 μm, is very versatile. It covers the absorption range of both dielectrics and many common metals, however, it is not optimal for highly reflective metals, such as copper. Due to these factors, the current slicing setup shown in figure 2(a) is limited to 2 mm wide filaments. Alternative laser technologies are definitely needed for realizing sub-millimeter wide filaments.

Fusion of the filament by the solder-reflow step is another key ingredient of the approach. The filaments are pressed together by pressure of the wire wrap and the winding pressure, but mechanical contact alone is unpredictable. Solder reflow prevents intrusion of epoxy between the filaments. Epoxy would introduce an isolation layer, thus defeating the purpose of an electrically coupled multifilamentary cable. Because the coupling does not increase the effective cable width, the re-flow step does not result in a higher magnetization loss. The most positive impact of the re-flow step is reduction of winding noise, which comes at the expense of 8% I_c reduction, figure 11. We do not observe the reduction in short, <20 cm, straight samples and the critical current density is very uniformly distributed throughout the coil, thus eliminating a possibility of an isolated defect.

4.2. Winding magnetization and flux jump stability

The AC loss measurements in 0.6 T field yielded the expected reduction of cyclic loss proportional to the filament width, figure 13. Due to the considerable hysteretic contribution, the coupling and eddy current loss were undetectable, which is typically the case for 2G conductors. By measuring the field hysteresis, we can also detect the field trapping after the

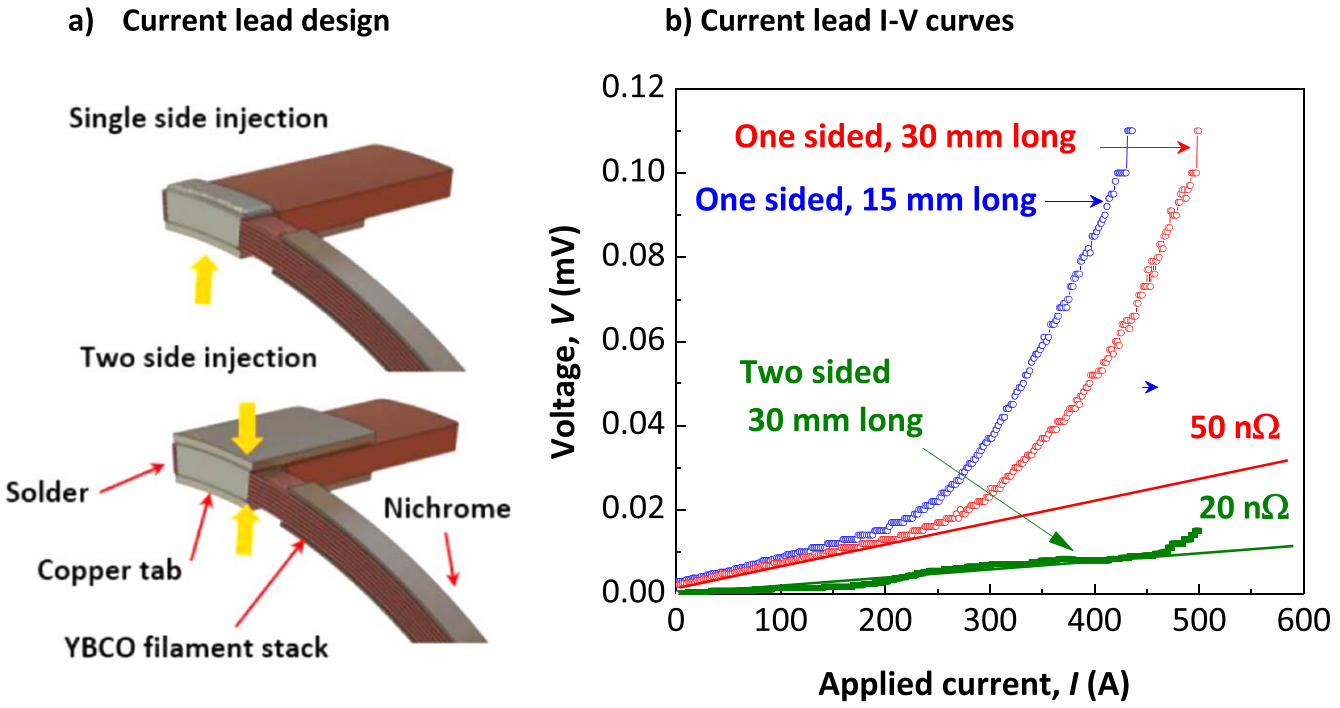

Figure 9. (a) Design of the current lead, showing a single-side injection (upper panel) and the double-side injection (lower panel) configurations. (b) *I–V* curves of various current lead configuration. Increasing the lead length yields only a marginal resistance reduction. Two-sided current injection allows reducing the lead resistance to 20 nΩ level. The straight lines represent linear fits of the low-current region of the *I–V* curve.

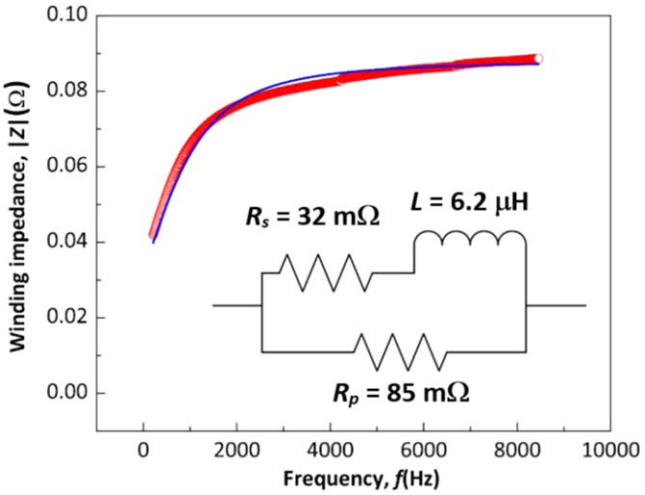

Figure 10. Frequency dependence of the winding impedance of the one-layer coil, coil C5. The inset shows the equivalent circuit used to fit the experimental data. The best fit, equation (2), is represented by the solid line.

zero-field cooldown and the subsequent flux penetration, figure 14(a). The maximum field on the winding generated by the coils used in the study exceeds the estimated penetration field of the cable ≈60 mT, and the 12 mm tape ≈10 mT, thus allowing for a fair comparison of the winding magnetization magnitude. In figure 14(b), the normalized hysteresis of the cable coil and a double pancake are compared. A simple argument can be used to show that at a given temperature the normalized field hysteresis is $\sim d$, where d is the filament width. This argument explains why the normalized hysteresis is approximately the same for coils with different inductance (see figure 14(b)). At 22 K, figure 14(c), the field created by the coil is too low to fully penetrate the winding, therefore the absolute value of hysteresis is lower. In summary, figure 14(b) demonstrates the advantage of narrow stacked filaments in reducing the winding magnetization and improving the field quality. Further improvement can be achieved by transposing the filaments. The current geometry is compatible only with a partial transposition, such as twisting. We will report the results of twisted cable tests in a forthcoming publication.

A finite element analysis of the trapped magnetic field distribution in a single layer coil along with the Hall probe location is presented in figure 15(a). Trapped field is generated by current loops in the outer turns of the coil, where the magnetic field reached the maximum penetration. The fits of the hysteresis data with the finite element model in figure 15(b) show reasonably good agreement with the experiment for partial hysteresis curves, such as 3d cycle. The model correctly predicts the absolute value of trapped field, but not the shape of the first cycle curve. This is most likely due to limitation of the axial symmetric geometry adopted in the simulation, which does not account for the cable non-uniformity. The results in figure 15(b) prove that the exfoliated filament stack can be modeled as a uniform slab using the averaged values of critical current density and transport current. This simplification allows for a reduction of the computation time and complexity when modeling a coil.

The high winding noise, figure 11, that we encountered in *as-wound* coils is a highly undesired development.

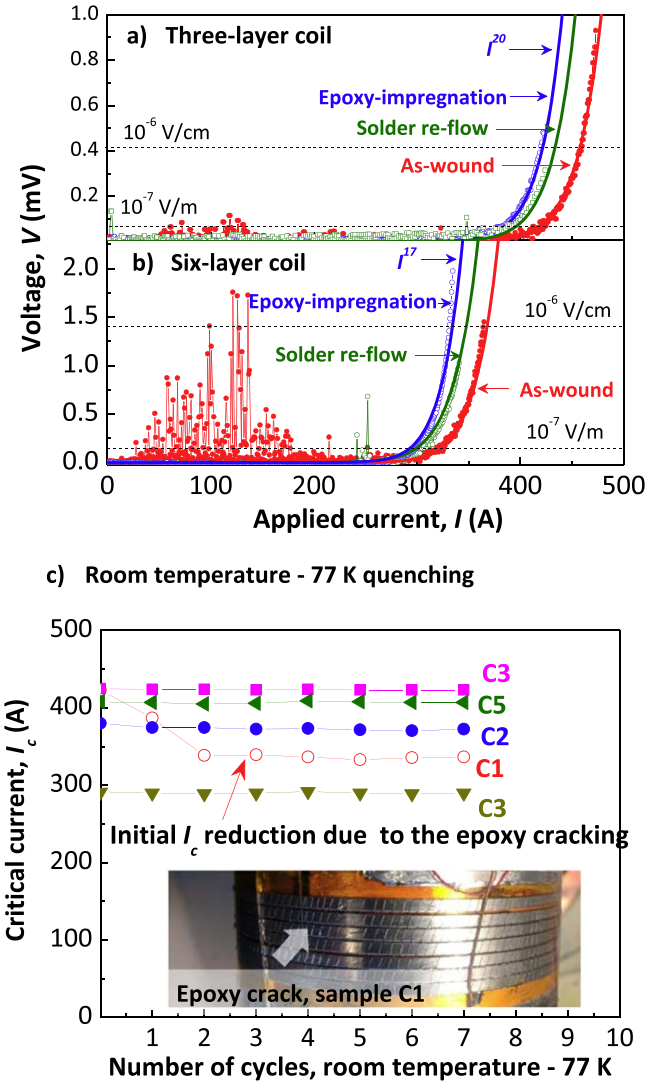

Figure 11. Effect of solder re-flow and epoxy impregnation on 77 K *I*–*V* curves of three-layer coil, C2 (a) and six-layer coil C3 (b). (c) Effect of room temperature −77 K cycling on critical current density. The inset shows epoxy cracking in a non-reinforced sample C1 which is responsible for the initial I_c reduction in sample C1.

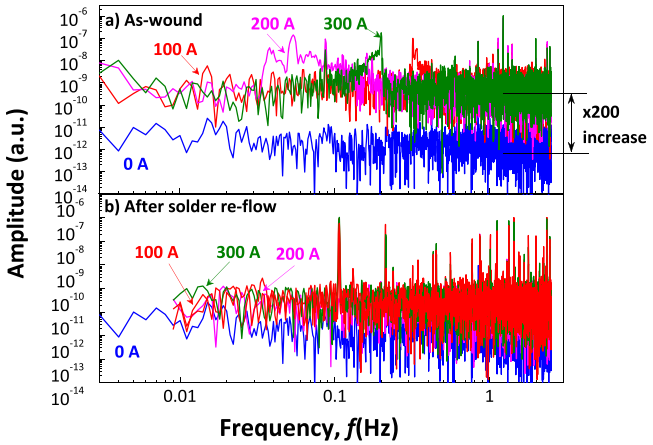

Figure 12. Fourier spectrum of the winding signal, coil C2, before the re-flow (a) and after the re-flow (b). Note a 200 times increase of the noise level in the as-wound coil after the current application.

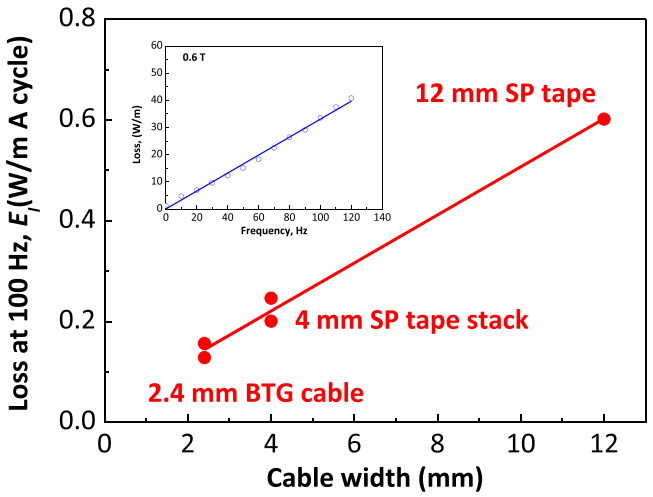

Figure 13. Summary of cyclic AC loss values at 0.6 T, 100 Hz, 77 K, normalized by the critical current. The results of 2.4 mm cable are compared with 4 and 12 mm wide SuperPower tape. The solid line is the linear approximation. The inset shows frequency dependence of AC loss of the 2.4 mm exfoliated cable at 0.6 T, 77 K. The linear approximation, presented as a solid line, indicates that the AC loss is purely hysteretic.

Reaching an amplitude as high as 10^{-6} V cm^{-1}, the noise would severely impede quench detection. The low-frequency parts of the noise spectrum, <1 Hz, figure 12(a), are especially difficult to filter without compromising the system response. We have established that the noise is an intrinsic electromagnetic phenomenon, not related to winding motion or an external signal interference. The most likely source is generation and collapse of weakly coupled shielding current loops involving several filaments that are in mechanical contact with each other. Due to the intermittent nature of a mechanical contact, the $\tau = L/R$ time constant of a loop can be very short. Indeed, taking inductance of one cable turn ≈0.2 μH, inter-filament resistance at 200 nΩ cm^2, we estimate the time constant of the loop decay at $\tau \approx 0.2$ s. Solder re-flow strongly bonds the filaments, thus suppressing the winding noise, at least under the experimental conditions of this study, as shown in figure 12(b). The voltage spikes on the *I*–*V* curve, figure 11(b), are strongly reminiscent of flux jumps effects, observed in Nb_3Sn [19, 20], but at much lower temperature, 4.2 K. The underlying mechanism of the winding noise is definitely similar: voltage generation by a rapid change of the winding magnetization. However, the current loops responsible for the winding noise in our 77 K experiments appear to be far weaker coupled, dissipating due to a short *L*/*R* time constant of the loop, rather than through the classic flux jump.

Even though electrically coupling the filaments seem to eliminate one source of flux instability, there is still an open question of stability of the cable with respect to low-field and self-field flux jumps. The flux jump stability is especially relevant for epoxy-impregnated conduction-cooled coils. In the conduction cooling regime, the heat transfer rate is much lower than in a liquid cryogen bath; for example, with 10 K

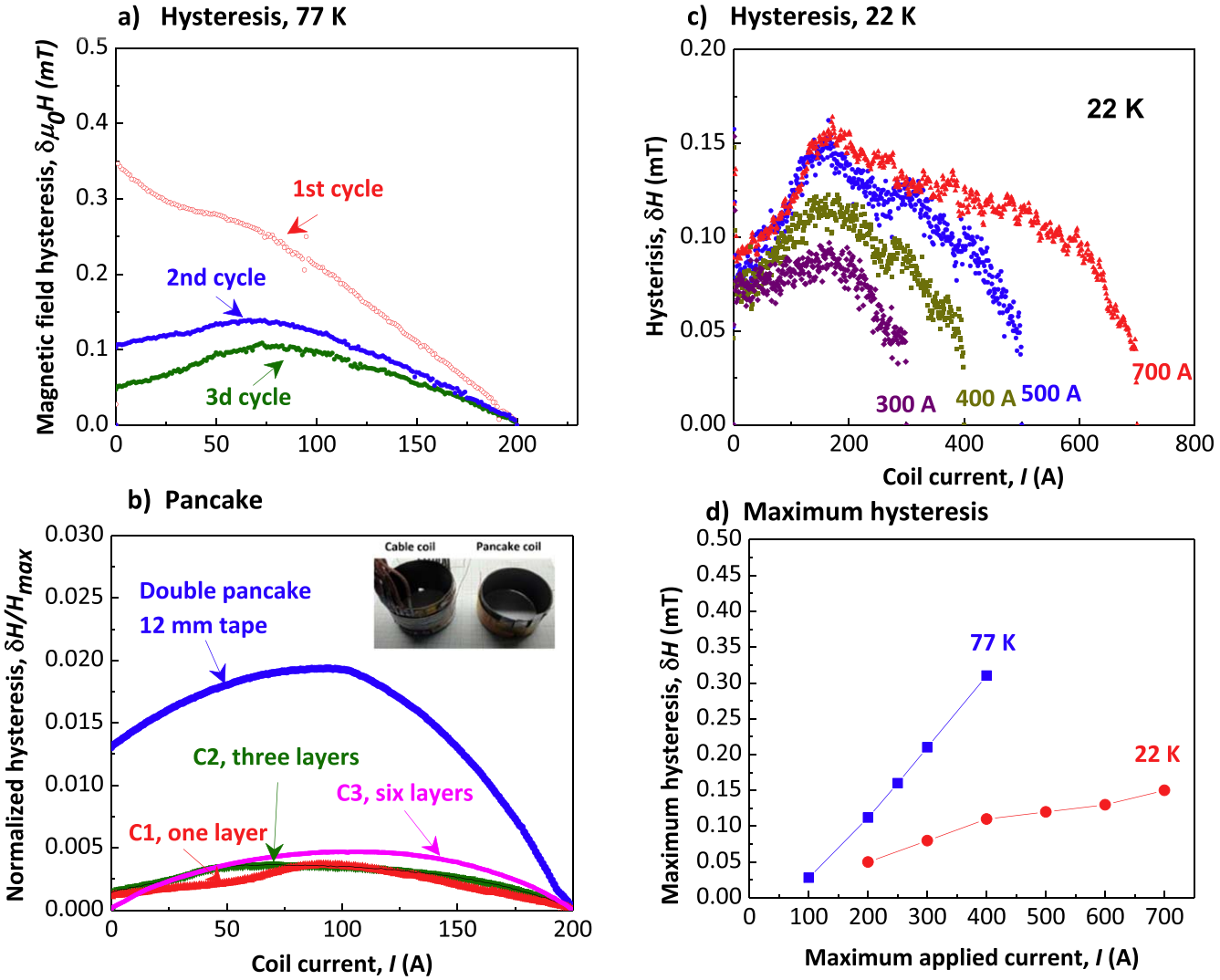

Figure 14. (a) Magnetic field hysteresis of sample C5, one-layer coil. Here 1st cycle means the cycle after the coil warm-up. The magnetic field is measured at 2 cm distance from the coil center. (b) Normalized hysteresis (3d cycle) of cable coils and compared with a double-pancake coil from 12 mm tape. The inset shows magnetically equivalent double pancake and a single layer cable coil. (c) Magnetic field hysteresis at 22 K, conduction-cooled mode.

temperature gradient only $\approx$0.25 W cm^{-2} can be evacuated by conduction through a 2 mm layer of epoxy, compared to approximately $\approx$1 W cm^{-2} in boiling helium at 4.2 K. Specific heat of common materials is severely reduced at 20 K and there is very little capacity to absorb heat released by the current loop collapse. Energy stored in an intra-filament current loop is $\sim d^2 I_c^2$, thus 2G-based conductors, with both high d and I_c, are expected to be particularly vulnerable to flux instabilities in locations with low $H||c$ (normal to the tape face) magnetic field component, where the winding magnetization is the highest. In order to estimate adiabatic stability of the cable in low field, we applied the flux jump model developed by Wilson [21]. Due to the extended spread between the operating temperature T and T_c a simple product, $C_p(T_c–T)$, in the original formula is replaced by an integral to account for a rapid rise of the specific heat of the winding, C_p at >30 K. Application of flux jump stability analysis predicts that the 2.4 mm cable would be stable down to liquid helium temperature, see figure 16. At the same time, a 10 mm wide tape might be susceptible to low-field flux instability at <30 K.

$$\beta(T) = \frac{\mu_0 J_e^2 a^2}{\gamma \int_{T_c}^{T} C_p dT}. \qquad (2)$$

Derivation of equation (2) assumes that heat, released by collapse of the shielding current loop is uniformly absorbed by the conductor. This is true for low-temperature materials, but unlikely for HTS where dissipation is often dominated by microscopic weak links. If the current loop collapse is caused by a spontaneous local dissipation event, which is confined to a narrow defect, the stability threshold would be significantly lower than the traditional $\beta = 3$ value. We conclude that the cable should be at least nominally stable down to helium temperature, which is in part supported by our 22 K experiments.

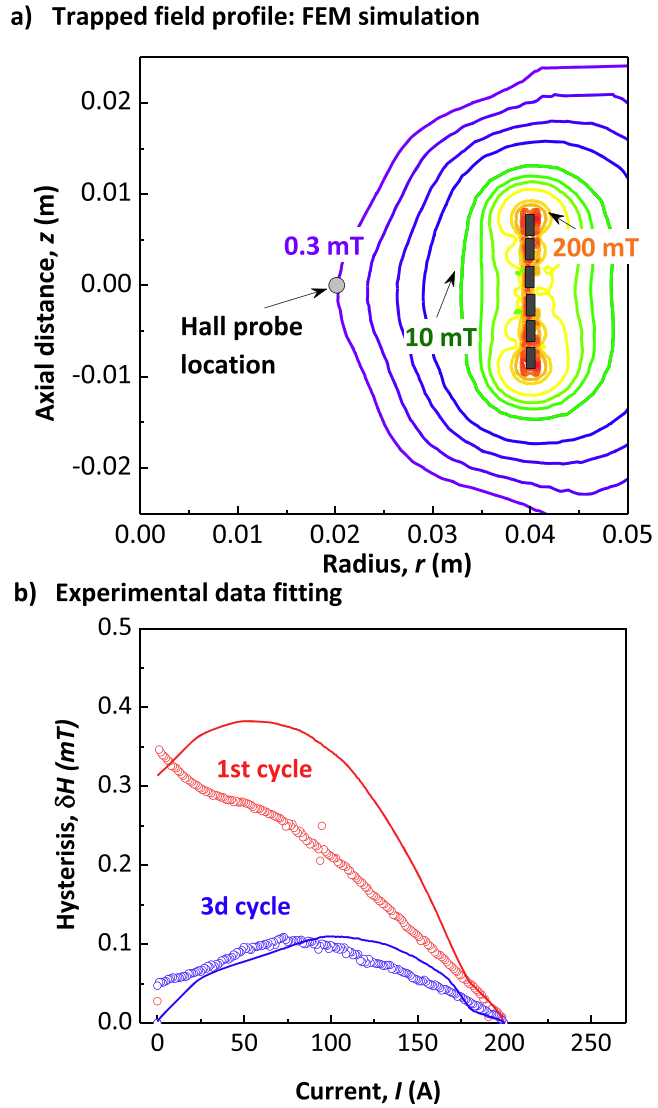

Figure 15. (a) Profile of the trapped field in a single layer coil after cycling to 200 A. A circle shows the Hall probe location. (b) Solid lines, approximation of the field hysteresis with the FEM model.

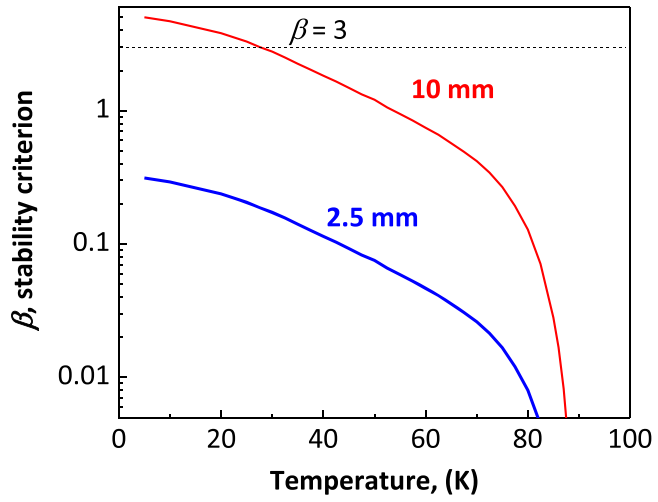

Figure 16. Flux stability criterion for a 10 mm tape and 2.5 mm cable, equation (2). The dotted line indicates $\beta = 3$ stability limit adopted by Wilson [21].

4.3. Thermal stress and mechanical stability of epoxy-impregnated winding

It is recognized that 2G conductors have low resistance to transverse pull [22], cleavage [23] and edge bending [24]. Therefore, 2G windings need to be secured by dense and bubble-free epoxy to prevent an accidental motion of filaments under Lorentz force loading or thermal contraction. Ideally, the cable should be compatible with a very low viscosity, <300 cP at 25 °C, epoxy, capable of penetrating a tight winding by wicking. The popular choice, glass filled epoxy Stycast 1251 has high viscosity >3000 cP at 25 °C, therefore is preferable to be used in a wet winding process. Wet winding does allow for post-winding heat treatment and filament fusion. Due to the difference in integrated linear expansion between 300 and 77 K, $\approx -280 \times 10^{-5}$ m/m for the winding and $\approx -600 \times 10^{-5}$ m/m for the epoxy impregnation [25], destructive stress can develop during the coil cooldown. The thermal stress can become problematic for impregnated 2G coils in two ways: (i) tensile yield strength of the epoxy might be exceeded, resulting in the epoxy cracking; (ii) transverse (radial) stress exceeds delamination strength of the YBCO-substrate interface or *c*-axis tensile strength of the YBCO layer. A finite element calculation shows that in our coil geometry, the axial stress reaches 50 MPa in the epoxy-impregnated volume areas surrounding the cable, thus exceeding the yield stress of Stycast 1266, 41 MPa. This explains the failure of sample C1 as seen in figure 11(c). Reinforcement of samples C2–C5 with 0.254 mm fiberglass increases the yield strength thus preventing the epoxy cracking even after multiple quenches to 77 K.

Separation of the YBCO layer from the substrate under radial stress is often cited as the primary cause of failure of epoxy-impregnated 2G coils [26–28]. Currently several approaches to degradation-free impregnation of 2G pancake coils, such as coil sectioning [29], coating or sleeving conductors, or compensation of the transverse stress by tension [30] have been developed and successfully tested. It is highly desirable, however, to retain good thermal contact between the epoxy and the winding. Therefore, introduction of a stress release agent would reduce the effective thermal conductivity of the winding pack. Our approach to the epoxy-compatible 2G cable is to eliminate the YBCO-substrate interface by exfoliation, secure the filaments with a high-strength wire wrap, and reduce the filament width. The pull stress depends on the filament width as $\sim d^2$, therefore the width reduction is especially effective in suppressing YBCO layer separation. In this work we show that the approach works at least for the 80 mm test coils. More recently we successfully manufactured and tested 160 mm epoxy-impregnated coils for a superconducting quadrupole.

5. Conclusion

In conclusion, performance of mini-coils wound from the eight-filament ExoCable™ was validated. The cable demonstrates compatibility with layer winding and impregnation

with low-viscosity epoxy, which are pre-requisites of a practical modern superconducting magnet. The solder re-flow step is shown to be essential for electrically bonding the filaments and suppressing the inductive noise of a coil. However, the re-flow also reduces the critical current density by 8%, on average. The re-flow process is expected to become more challenging for larger magnets due to greater thermal inertia and inevitable thermal gradients. A possible solution is rapid localized heating of the cable that would locally melt the solder within several seconds, thus avoiding prolong exposure of the superconducting filament to the molten solder. Epoxy chemistries with low thermal expansion are expected to further improve the critical current retention after the impregnation step.

Acknowledgments

The work at Brookhaven Technology Group was supported by the Department of Energy, Office of High Energy Physics under SBIR Phase II award DE-SC0013856. The authors wish to thank Martin Rupich of American Superconductor Corporation for providing the 2G wire coupons, Chung-Chueh Chang of Stony Brook University for scanning electron microscopy and DSC measurements. MM and ZM wish to thank the Office of Strategic Partnership for Industrial Resurgence at Stony Brook University for financial support.

ORCID iDs

Vyacheslav Solovyov https://orcid.org/0000-0003-1879-9802

References

[1] Rupich M W, Xiaoping L, Sathyamurthy S, Thieme C L H, DeMoranville K, Gannon J and Fleshler S 2013 Second generation wire development at AMSC *IEEE Trans. Appl. Supercond.* **23** 6601205

[2] Zhang Y F, Lehner T F, Fukushima T, Sakamoto H and Hazelton D W 2014 Progress in production and performance of second generation (2G) HTS wire for practical applications *IEEE Trans. Appl. Supercond.* **24** 7500405

[3] Iwai S, Miyazaki H, Tosaka T, Tasaki K, Urata M, Ioka S and Ishii Y 2013 A 5.9 Tesla conduction-cooled coil composed of a stack of four single pancakes wound with YBCO wide tapes *Physica* C **494** 203–7

[4] Trillaud F, Palanki H, Trociewitz U P, Thompson S H, Weijers H W and Schwartz J 2003 Normal zone propagation experiments on HTS composite conductors *Cryogenics* **43** 271–9

[5] Kwanglok K, Kwangmin K, Kabindra R B, Kyle R, Jae Young J, Young Jin H, SangGap L, Sangwon Y and Seungyong H 2017 Quench behavior of a no-insulation coil wound with stainless steel cladding REBCO tape at 4.2 K *Supercond. Sci. Technol.* **30** 075001

[6] Sangwon Y, Jaemin K, Hunju L, Seungyong H and Seung-Hyun M 2016 26 T 35 mm all-GdBa$_2$ Cu$_3$O$_{7-x}$ multi-width no-insulation superconducting magnet *Supercond. Sci. Technol.* **29** 04LT04

[7] Takayasu M, Chiesa L, Allen N C and Minervini J V 2016 Present status and recent developments of the twisted stacked-tape cable conductor *IEEE Trans. Appl. Supercond.* **26** 25–34

[8] Wolf M J, Bagrets N, Fietz W H, Lange C and Weiss K 2018 Critical current densities of 482 A mm^{-2} in HTS crossconductors at 4.2 K and 12 T *IEEE Trans. Appl. Supercond.* **28** 4802404

[9] Weiss J D, Mulder T, ten Kate H and van der Laan D 2017 Introduction of CORC ® wires: highly flexible, round high-temperature superconducting wires for magnet and power transmission applications *Supercond. Sci. Technol.* **30** 014002

[10] Goldacker W, Grilli F, Pardo E, Kario A, Schlachter S and Vojenčiak M 2014 Roebel cables from REBCO coated conductors: a one-century-old concept for the superconductivity of the future *Supercond. Sci. Technol.* **27** 093001

[11] Kim J H, Kim C H, Pothavajhala V and Pamidi S V 2013 Current sharing and redistribution in superconducting DC cable *IEEE Trans. Appl. Supercond.* **23** 4801304

[12] Solovyov V and Farrell P 2017 Exfoliated YBCO filaments for second-generation superconducting cable *Supercond. Sci. Technol.* **30** 014006

[13] Murphy J P, Mullins M J, Barnes P N, Haugan T J, Levin G A, Majoros M, Sumption M D, Collings E W, Polak M and Mozola P 2013 Experiment setup for calorimetric measurements of losses in HTS coils due to AC current and external magnetic fields *IEEE Trans. Appl. Supercond.* **23** 4701505

[14] Mark D A, Rodriguez-Zermeno V M, Hong Z, Yuan W, Flack T J, Coombs T A *et al* 2011 An improved FEM model for computing transport AC loss in coils made of RABiTS YBCO coated conductors for electric machines *Supercond. Sci. Technol.* **24** 045005

[15] Schaaf P 2010 *Laser Processing of Materials : Fundamentals, Applications and Developments* (*Springer Series in Materials Science*) vol 231 (Berlin: Springer)

[16] Lee N-C 2001 *Reflow Soldering Processes* ed N-C Lee (Burlington, VT: Newnes)

[17] Francesco G and Anna K 2016 How filaments can reduce AC losses in HTS coated conductors: a review *Supercond. Sci. Technol.* **29** 083002

[18] Kesgin I, Majkic G and Selvamanickam V 2013 Fully filamentized HTS coated conductor via striation and selective electroplating *Physica* C **486** 43–50

[19] Bordini B *et al* 2006 Voltage spikes in Nb$_3$Sn and NbTi strands *IEEE Trans. Appl. Supercond.* **16** 366–9

[20] Ghosh A K, Cooley L D and Moodenbaugh A R 2005 Investigation of instability in high J_c Nb$_3$Sn strands *IEEE Trans. Appl. Supercond.* **15** 3360–3

[21] Wilson M N 1983 Superconducting magnets *Monographs on Cryogenics* (Oxford: Clarendon) p 335

[22] Laan D C v d, Ekin J W, Clickner C C and Stauffer T C 2007 Delamination strength of YBCO coated conductors under transverse tensile stress *Supercond. Sci. Technol.* **20** 765

[23] Yanagisawa Y, Nakagome H, Takematsu T, Takao T, Sato N, Takahashi M and Maeda H 2011 Remarkable weakness against cleavage stress for YBCO-coated conductors and its effect on the YBCO coil performance *Physica* C **471** 480–5

[24] Kajita K, Takao T, Maeda H and Yanagisawa Y 2017 Degradation of a REBCO conductor due to an axial tensile stress under edgewise bending: a major stress mode of deterioration in a high field REBCO coil's performance *Supercond. Sci. Technol.* **30** 074002

[25] Cryogenic Technology Resources database (National Institute for Standards and Technology) https://trc.nist.gov/cryogenics/
[26] Matsuda T, Okamura T, Hamada M, Matsumoto S, Ueno T, Piao R, Yanagisawa Y and Maeda H 2018 Degradation of the performance of an epoxy-impregnated REBCO solenoid due to electromagnetic forces *Cryogenics* **90** 47–51
[27] Shin H J, Kim K L, Choi Y H, Kwon O J, Hahn S, Iwasa Y and Lee H G 2013 Effects of impregnating materials on thermal and electrical stabilities of the HTS racetrack pancake coils without turn-to-turn insulation *IEEE Trans. Appl. Supercond.* **23** 7700404
[28] Takematsu T, Hu R, Takao T, Yanagisawa Y, Nakagome H, Uglietti D, Kiyoshi T, Takahashi M and Maeda H 2010 Degradation of the performance of a YBCO-coated conductor double pancake coil due to epoxy impregnation *Physica* C **470** 674–7
[29] Miyazaki H, Iwai S, Tosaka T, Tasaki K and Ishii Y 2014 Degradation-free impregnated YBCO pancake coils by decreasing radial stress in the windings and method for evaluating delamination strength of YBCO-coated conductors *IEEE Trans. Appl. Supercond.* **24** 4600905
[30] Liu L Y, Chen W, Zhang H Y, Yang X S, Yang Y, Zhang Y and Zhao Y 2017 Effect of winding tension, support material, and epoxy impregnation on the strain and critical current of YBCO coil *IEEE Trans. Appl. Supercond.* **27** 8400507